Geophys. J. Int. (2000) **143,** 204–218

Inversion of two-dimensional numerical convection experiments for a fluid with a strongly temperature-dependent viscosity

Frédéric Deschamps* and Christophe Sotin

Laboratoire de planétologie et géodynamique, Université de Nantes, 2 *rue de la Houssinière,* BP 92208, 44322 *Nantes cedex* 3, *France*

Accepted 2000 May 16. Received 2000 April 20; in original form 1999 August 5

SUMMARY

2-D thermal convection numerical experiments are conducted for a fluid with an infinite Prandtl number, a strongly temperature-dependent viscosity, and isothermal horizontal boundaries. The core Rayleigh number ($Ra_{\bar{\theta}}$), determined with the temperature of the well-mixed interior, is in the range $5\times10^5 < Ra_{\bar{\theta}} < 2\times10^7$, and the ratio of the top to the bottom viscosity ($\Delta\mu$) can be as large as $\Delta\mu = 10^6$. Different convective regimes are possible, depending on the values of $Ra_{\bar{\theta}}$ and $\Delta\mu$. This paper focuses on the conductive-lid regime, in which convection is confined to a sublayer. First, a least-squares fit of more than 40 numerical experiments suggests that the temperature difference across the lower thermal boundary layer (ΔT_1) depends mostly on the viscous temperature scale (ΔT_v) defined by Davaille & Jaupart (1993), and slightly on the temperature difference across the fluid layer (ΔT): $\Delta T_1 = 1.43\Delta T_v - 0.03\Delta T$. Second, a generalized non-linear inversion of the data does not support the assumptions that the temperature difference across the upper boundary layer is proportional to ΔT_v, and that isoviscous scaling laws can be used for describing heat flux through the convective sublayer. Third, a generalized non-linear inversion of the data is carried out in order to avoid any assumptions on the parameters. This leads to the following heat flux scaling law: $Nu = 3.8(\Delta T_v/\Delta T)^{1.63} Ra_{\bar{\theta}}^{0.258}$, where the Nusselt number (Nu) is the non-dimensional heat flux. This scaling law is different from that proposed by previous studies. It reproduces the data at better than 1 per cent and fits the results of previous numerical experiments very well (e.g. Christensen 1984).

Finally, a thermal boundary layer analysis is performed. For a fluid heated from below, the upper and lower thermal boundary layers interact with one another, inducing a thermal erosion of the conductive lid. This study suggests that the dynamics of convection is driven by the instability of the lower thermal boundary layer. Therefore, an alternative way to determine the heat flux is to use the value of the lower thermal boundary layer Rayleigh number (Ra_δ). This value is not independent of $Ra_{\bar{\theta}}$, unlike the case for an isoviscous fluid. A least-squares fit of the data leads to $Ra_\delta = 0.28 Ra_{\bar{\theta}}^{0.21}$. This law provides a very convenient way to model the thermal evolution of planetary mantles.

Key words: heat transfer, scaling law, temperature-dependent viscosity, thermal convection.

1 INTRODUCTION

The thermal history of Earth-like planets is controlled by the efficiency of heat transfer through planetary mantles (e.g. Schubert *et al.* 1979; Stevenson *et al.* 1983). Since it is believed that Earth-like planets were composed of an iron-rich liquid core surrounded by a solid convective mantle just after accretion, the rate of heat transfer through the mantle will drive the rate of cooling of the liquid core. Convection in the mantle is generally described by an upper thermal boundary layer where instabilities form and sink, and a lower thermal boundary layer where hot instabilities grow and rise. The heat is transferred by conduction through both boundary layers. In between these two boundary layers, the convective fluid is nearly adiabatic. The thermal history of planets can be described if laws relating heat flux and mean temperature to the vigour of convection are established with the appropriate boundary conditions and fluid properties.

* Temporarily at: Faculty of Earth Sciences, University of Utrecht, PO Box 80.021, Budapestlaan 4, 3508 TA Utrecht, The Netherlands. E-mail: deschamp@geo.uu.nl

The efficiency of convection can be described by the Nusselt number, which is the ratio of the surface mean heat flux to the conductive heat flux without convection. For an isoviscous fluid, linear stability analysis (e.g. Turcotte & Oxburgh 1967) predicts that the Nusselt number is a power law of the Rayleigh number (Ra) with an exponent equal to 1/3. The Rayleigh number is a measurement of the vigour of convection, and is given by

$$Ra = \alpha \rho g \Delta T b^3 / \mu \kappa , \quad (1)$$

where α is the coefficient of thermal expansion, ρ the density, g the acceleration of gravity, ΔT the temperature difference across the fluid, b the thickness of the fluid layer, μ the viscosity, and κ the thermal diffusivity. Numerical studies have indeed shown that the Nusselt number is a power law of the Rayleigh number with an exponent close to 1/3 (Table 1).

Howard (1966) pointed out that a thermal boundary layer becomes unstable if its thickness (δ) exceed a certain value which is determined by the thermal boundary layer Rayleigh number (Ra_δ):

$$Ra_\delta = \alpha \rho g (\delta T) \delta^3 / \mu \kappa , \quad (2)$$

where δT is the temperature difference across the thermal boundary layer. The value of Ra_δ depends on whether the boundaries are free-slip boundaries or rigid boundaries (Roberts 1979; Frick *et al.* 1983). The Nusselt number can therefore be described as

$$Nu = \left(\frac{\delta T}{\Delta T} \right)^{4/3} \left(\frac{Ra}{Ra_\delta} \right)^{1/3} , \quad (3)$$

$$Nu = a\, Ra^\beta . \quad (4)$$

Such laws have previously been applied to describe the thermal history of planets (e.g. Stevenson *et al.* 1983; Schubert & Spohn 1992). These studies used eq. (3) with a constant value of Ra_δ, which is equivalent to using eq. (4) with $\beta = 1/3$. Planetary mantles are, however, far from being equivalent to the Rayleigh–Bénard case. Among the most important differences are the mode of heating (Parmentier *et al.* 1994; Sotin & Labrosse 1999) and the viscous properties of the fluid (Christensen 1984; Davaille & Jaupart 1993; Solomatov 1995; Moresi & Solomatov 1995; Grasset & Parmentier 1998).

Viscosity controls the amount of deformation supported by a rock submitted to a given stress. Within planetary mantles, it varies by several orders of magnitude due to temperature and pressure variations. For most materials, including the minerals of the Earth's mantle, the deformation rate is a thermally activated process that depends strongly on temperature and, to a weaker extent, on pressure. In a Newtonian fluid, the deformation rate varies linearly with differential stress. As a result, viscosity does not depend on differential stress. Most studies that have investigated the effect of variable viscosity have considered a Newtonian fluid. The debate on whether the viscosity of the mantle is Newtonian or not is still open. Other complexities may arise due to the presence of fluids (mainly water and CO_2), which may weaken the rock (e.g. Chopra & Paterson 1984; Karato *et al.* 1986). Although pressure, differential stress and the presence of fluids may affect the value of viscosity, it is considered that viscosity is most sensitive to temperature variations. Laboratory experiments (Booker & Stengel 1978; Richter *et al.* 1983; Davaille & Jaupart 1993) and analytical and numerical models (Christensen 1984; Morris & Canright 1984; Ogawa *et al.* 1991; Solomatov 1995; Moresi & Solomatov 1995) have shown that a fluid submitted to strong viscosity variations separates into an upper cold, rigid lid where viscosity is high, and a convective sublayer where viscosity variations are small. Within the upper lid, heat is transferred by conduction. Therefore, the value of the Nusselt number decreases with increasing values of the viscosity contrast ($\Delta\mu$), defined as the ratio of the surface viscosity to the bottom viscosity:

$$\Delta\mu = \mu_0 / \mu_1 . \quad (5)$$

The 2-D numerical work of Christensen (1984) shows clearly that the logarithmic slope β (eq. 4) depends on the viscosity contrast. Moreover, he finds that the slope varies with the value of the Rayleigh number. These features suggest that different regimes of convection occur, depending on Ra and $\Delta\mu$. Solomatov (1995) distinguishes three domains. For a viscosity contrast lower than 10^2, the effect of viscosity variations is small and the fluid behaves almost as an isoviscous fluid. The second regime corresponds to the so-called 'lid regime', and occurs for viscosity contrasts larger than 10^4. Finally, a transitional regime occurs for viscosity contrasts between 10^2 and 10^4.

For a fluid heated from within, there is only one thermal boundary layer, at the top of the fluid. The study of Davaille & Jaupart (1993) showed that the temperature variation across this layer (ΔT_e) is proportional to a viscous temperature

Table 1. Scaling laws for the heat flux, in the case of an isoviscous fluid. Various boundary conditions are considered: F/F: top and bottom boundaries are free-slip; F/R: top is free-slip and bottom is rigid; R/F: top is rigid and bottom is free-slip; R/R: top and bottom boundaries are rigid. The aspect ratio is equal to 1, except for the study of Kvernvold (1979), where $r_a = 1.2$.

Reference	Ra range	a	β	Boundary conditions
Linear stability analysis	–	0.294	1/3	F/F
Jarvis & Peltier (1982)	$4.10^4 - 8.10^6$	0.279	0.313	F/F
Christensen (1984)	$10^4 - 10^7$	0.2697	0.3185	F/F
Schubert & Anderson (1985)	$8.10^4 - 8.10^7$	0.268	0.319	F/F
Hansen & Yuen (1993)	$10^4 - 10^{11}$	0.250	0.323	F/F
Kvernvold (1979)	$3.10^3 - 5.10^4$	0.195	0.3	F/R
Frick *et al.* (1983)	$3.10^4 - 7.10^4$	0.332	0.225	R/R
This study	$10^4 - 10^6$	0.258	0.321	F/F
	–	0.336	0.252	R/F
	–	0.339	0.223	R/R

scale (ΔT_v):

$$\Delta T_e = c\Delta T_v , \tag{6}$$

$$\Delta T_v = -\frac{\mu(\bar{T})}{d\mu/dT(\bar{T})} , \tag{7}$$

where $\bar{T}$ is the mean temperature of the well-mixed interior. Davaille & Jaupart (1993) found $c = 2.24$. 2-D numerical studies are in very good agreement with this value (Grasset & Parmentier 1998), although the viscous laws are different. Eqs (6) and (7) imply that the viscosity contrast across the thermal boundary layer is constant. Moreover, they allow for the determination of the lid thickness, assuming the continuity of heat flux between the top of the thermal boundary layer and the bottom of the conductive lid. In the Rayleigh–Bénard case, the 2-D numerical work of Moresi & Solomatov (1995) suggests the following scaling relations:

$$Nu = 1.89\,\frac{Ra_i^{0.2}}{p^{1.02}} , \tag{8}$$

$$\Delta T_{bot} = \frac{1.10}{p^{0.73} Ra_i^{0.04}} , \tag{9}$$

$$p = \frac{\Delta T}{\Delta T_v} , \tag{10}$$

where p describes the temperature dependence of viscosity, ΔT_{bot} is the temperature variation across the lower thermal boundary layer, and Ra_i is the core Rayleigh number, defined with the viscosity of the well-mixed interior. To obtain the scaling law for heat flux, Moresi & Solomatov (1995) fixed the Rayleigh number exponent to a theoretical value of 0.2 (Morris & Canright 1984; Solomatov 1995). We note, however, that the scaling law for the Nusselt number does not provide a good fit for the numerical data of Christensen (1984) (Fig. 1).

The initial aim of the present study is to use generalized non-linear inversion theory (Tarantola & Valette 1982) to determine scaling laws such as (8) and (9). This leads us to conduct 2-D numerical work in the conductive-lid regime. Numerical data ($\bar{T}$, Nu) are then inverted, and results are discussed using a thermal boundary layer analysis. For the range of Rayleigh number and viscosity contrast investigated in the present study, it is found that the temperature across the lower thermal boundary layer depends linearly on the viscous temperature scale. A scaling relation for the Nusselt number is found and gives a good fit for Christensen's results. In addition, this study suggests that convection is driven by instabilities in the lower thermal boundary layer, and that isoviscous scaling laws cannot be used to describe heat transfer in the convective sublayer.

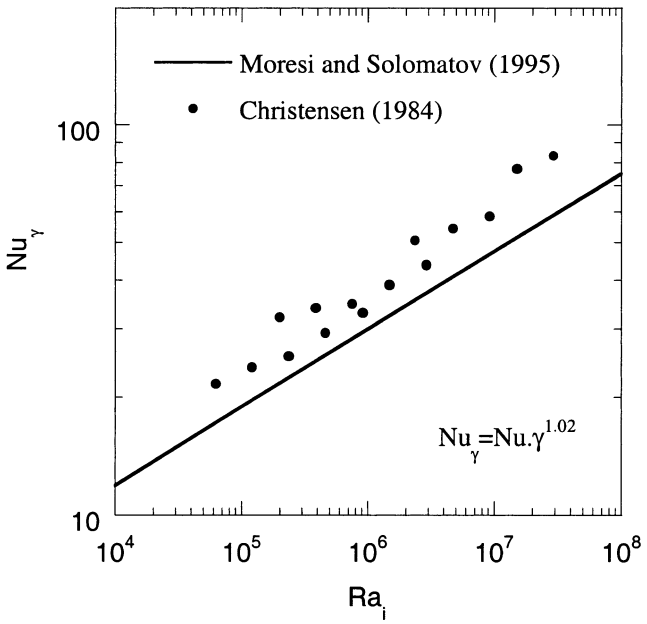

Figure 1. Comparison between the results of Christensen (1984) and the scaling law for heat flux suggested by Moresi & Solomatov (1995).

2 THE NUMERICAL MODEL

2.1 Equations

We solved the equations of convection for a Newtonian fluid in a 2-D Cartesian box. The fluid is assumed to have an infinite Prandtl number, and to verify the Boussinesq approximation. These assumptions lead to the following equations for conservation of momentum, mass and energy:

$$\frac{\partial \tau_{ij}}{\partial x_j} - \frac{\partial P}{\partial x_i} = -\alpha \rho g T e_i , \tag{11}$$

$$\frac{\partial u_i}{\partial x_i} = 0 , \tag{12}$$

$$\rho C_P \frac{\partial T}{\partial t} = k\overline{\nabla}^2 T - u_i \frac{\partial T}{\partial x_i} , \tag{13}$$

where x_i, u_i and e_i are the components of the position, velocity and vertical unit vectors, P and T are pressure and temperature perturbations, C_P is the heat capacity at constant pressure, and τ_{ij} is the deviatoric stress tensor.

The box is heated from below and cooled on the top. This is done by fixing the surface and bottom temperatures, respectively, to T_0 and $T_1 = T_0 + \Delta T$. Internal energy sources are neglected. To avoid lateral heat loss, we impose a zero heat flux on vertical edges. Since the total mass is conserved, the normal velocities on the boundaries must be zero. Finally, we impose free-slip boundary conditions on all boundaries.

In the present work, the viscosity is strongly temperature-dependent, and follows a simple exponential law:

$$\mu(T) = \mu_{ref} \exp\left[-\gamma \frac{(T - T_{ref})}{\Delta T}\right] , \tag{14}$$

where T_{ref} is a reference temperature, μ_{ref} is the viscosity at this temperature, and γ is a constant. Eq. (14) implies that γ is equal to the parameter p in eqs (8) to (10). In addition, γ is linked to the ratio of the top viscosity to the bottom viscosity ($\Delta\mu$):

$$\gamma = \ln(\Delta\mu) . \tag{15}$$

Eqs (11) to (13) are non-dimensionalized using the box's depth b for the length-scale, b^2/κ for the timescale, κ/b for the velocity-scale, and ΔT for the temperature-scale. The body force (right-hand term of eq. 11) is then given as a function of the Rayleigh number. A second non-dimensional parameter, which takes the viscosity variations into account, must be defined. In our study, we will use the parameter γ.

2.2 Choice of the Rayleigh number

The Rayleigh number depends on the viscosity. Viscosity varies throughout the fluid. To discuss the results, it is therefore necessary to define a reference Rayleigh number associated with a reference viscosity. For instance, the surface Rayleigh number (Ra_0), which is useful in understanding the onset of cold instabilities in the top thermal boundary layer, is calculated with the viscosity at $T=T_0$.

Some authors have presented their results as a function of a Rayleigh number $Ra_{1/2}$ calculated with the viscosity at $T_{1/2}=\Delta T/2$ (e.g. Richter *et al.* 1983; Christensen 1984). This definition is not well suited to a fluid with strong viscosity variations, since the mean temperature of the well-mixed interior is always greater than $T_{1/2}$. However, this definition will be used to make comparisons with previous studies.

In the present study, the core Rayleigh number ($Ra_{\bar{\theta}}$) is used. The viscosity is computed at the temperature of the well-mixed interior ($\bar{T}$), which is well approximated by the horizontally averaged temperature at mid-depth:

$$\bar{T}\sim T_{z=b/2}=\frac{1}{L}\int_0^L T(x,\, z=b/2)\,dx\,, \tag{16}$$

where L is the length of the box. The volumetric averaged temperature of the well-mixed interior differs from the value computed by eq. (16) by less than a few per cent. This definition of the core Rayleigh number is equivalent to the definition of Ra_i used by Moresi & Solomatov (1995).

Given the temperature distribution and the viscosity law, it is simple to calculate the relation between the Rayleigh numbers at two distinct points. For an exponential viscosity law (eq. 14), the relation between the core and surface Rayleigh numbers is

$$Ra_{\bar{\theta}}=Ra_0\exp(\gamma\bar{\theta})\,. \tag{17}$$

Similarly, $Ra_{1/2}$ is given by

$$Ra_{1/2}=Ra_0\exp(\gamma/2)\,. \tag{18}$$

2.3 Algorithm

Calculations are made on uniform staggered grids. This structure is well adapted to the resolution of primitive variables (velocities and pressure). The scalar quantities (temperature and pressure) are calculated in the centre of each cell, whereas the vertical (horizontal) velocities are determined on the top and on the bottom (lateral sides) of each cell.

The resolution of the energy equation is a simple time relaxation. Problems arise from the non-linear advective term, $u_i=\partial T/\partial x_i$, which induces artificial transport in incorrect directions. To avoid such disturbances, we have used an upwind scheme well adapted to high Peclet numbers (Spalding 1972).

The momentum equation is solved by an alternate direction implicit (ADI) relaxation method. The resolution of this equation directly on the finest grid is, however, very expensive in cpu time. To speed up the convergence, we have used a multigrid method, fully described by Stüben & Trottenberg (1982). This method is efficient at solving for the non-dimensional form of eq. (11), even for high viscosity ratios (Sotin *et al.* 1995).

The mean heat flux at depth z is given as

$$\bar{q}(z)=\frac{1}{L}\int_0^L\left(\frac{\partial T}{\partial z}-\rho C_P u_z T\right)dx\,. \tag{19}$$

The Nusselt number (Nu), which is the ratio between $\bar{q}$ and the conductive heat flux $q_c=k\Delta T/b$, measures the efficiency of convection. If there is no internal heating, the convective heat flux (and so the Nusselt number) must be constant with depth.

2.4 Precision of the calculations

The calculated Nusselt number and the non-dimensional temperature of the well-mixed interior have a range of uncertainty, respectively σ_{Nu} and $\sigma_{\bar{\theta}}$. There are two kinds of errors. First, the stationary state is only reached for an infinite time. Therefore, the accuracy of numerical solutions depends on the elapsed time. A good convergence test is given by the variation of the core temperature. A converged state is obtained when $\bar{\theta}$ is no longer evolving. At time step i, the uncertainties on $\bar{\theta}$ and Nu due to convergence are given by

$$\sigma_{c,\bar{\theta}}=\left|\frac{\bar{\theta}_i-\bar{\theta}_{i-1}}{\bar{\theta}_{i-1}}\right| \quad\text{and}\quad \sigma_{c,Nu}=\left|\frac{Nu_i-Nu_{i-1}}{Nu_{i-1}}\right|. \tag{20}$$

In our experiments, the calculations are stopped when $|\bar{\theta}-\bar{\theta}_{i-1}|\le 10^{-5}$, which usually implies that $|Nu_i-Nu_{i-1}|\le 10^{-3}$. In some cases (usually for high Rayleigh numbers), the solutions are time-dependent: the solution has converged, but the mean temperature oscillates around a stationary value. For such cases, mean fields must be computed over a significant time interval (usually several pseudo-periods), leading to an uncertainty equal to the maximal variations of the parameters (temperature and Nusselt number).

Second, errors arise from the limited resolution of the grid. For numerical accuracy, it is desirable that at least three points describe each thermal boundary layer. However, the limitation in the computing time is such that calculations cannot be performed on grids larger than 64×64 grid points. In Table 2, we have reported the Nusselt number, the core temperature, the maximum of the top and bottom horizontal velocities, and the quadratic velocity for various resolutions of the grid. Extrapolated values can be deduced from these results, and used to estimate the error arising from the limited resolution of the uniform grid spacing:

$$\sigma_{r,\bar{\theta}}=\left|\frac{\bar{\theta}_{extra}-\bar{\theta}_N}{\bar{\theta}_{extra}}\right| \quad\text{and}\quad \sigma_{r,Nu}=\left|\frac{Nu_{extra}-Nu_N}{Nu_{extra}}\right|, \tag{21}$$

where the subscripts 'extra' and 'N' indicate the extrapolated and $N\times N$ grid-point values, respectively. The grid size used in the present study is such that $\sigma_{r,\bar{\theta}}$ is less than 0.5 per cent and $\sigma_{r,Nu}$ is less than 2–3 per cent.

The scaling law of the Nusselt number for isoviscous fluids has been compared with those reported in previous studies. Our values are in close agreement with these studies, whatever the boundary conditions (Table 1). We have also compared our results with those of Christensen (1984). In Fig. 2, the Nusselt numbers are plotted as a function of $Ra_{1/2}$. Our results for $\Delta\mu=10^3$ are identical to those of Christensen (1984). We cannot make a direct comparison for the other viscosity ratios because they are different. However, the results are consistent. For example, the results of Christensen for a viscosity ratio of 64 give slightly higher values of the Nusselt number than those obtained here for a viscosity ratio of 100.

Table 2. Accuracy of some observables as a function of the grid definition. Nu is the Nusselt number, $\bar{\theta}$ the core temperature, U_0 and U_1 the maximum surface and bottom velocities, respectively, and U_q the root-mean-square velocity. An extrapolated value is determined for each parameter. These extrapolated values are used as a reference to compute the relative errors (number in %) of individual results. The viscosity ratio is equal to 10^4 for all calculations.

$Ra_{1/2}$	Grid size	Nu	$\bar{\theta}$	$U_0^{(1)}$	$U_1^{(1)}$	U_q
10^4	32×32	2.625	0.8738	2.703	−183.7	76.05
		2.3%	0.36%	1.2%	2.4%	1.2%
–	48×48	2.652	0.8752	2.691	−182.3	76.49
		1.3%	0.21%	0.71%	1.6%	0.66%
–	64×64	2.662	0.8758	2.686	−181.4	76.65
		1.0%	0.13%	0.52%	1.1%	0.45%
–	96×96	2.669	0.8761	2.683	−180.7	76.77
		0.7%	0.10%	0.41%	0.72%	0.30%
–	128×128	2.672	0.8763	2.680	−180.4	76.82
		0.6%	0.08%	0.30%	0.56%	0.23%
–	Extrapolation	2.688	0.877	2.672	−179.4	77.00
10^5	32×32	4.999	0.8629	22.76	−757.6	355.9
		4.8%	1.6%	7.1%	5.1%	2.2%
–	48×48	5.107	0.8686	22.01	−751.1	355.5
		2.7%	0.96%	3.6%	4.2%	2.1%
–	64×64	5.151	0.8712	21.73	−741.2	353.1
		1.9%	0.66%	2.3%	2.8%	1.4%
–	96×96	5.188	0.8737	21.52	−731.8	351.1
		1.2%	0.38%	1.3%	1.5%	0.80%
–	128×128	5.203	0.8747	21.44	−727.9	350.3
		0.9%	0.26%	0.89%	0.96%	0.57%
–	Extrapolation	5.250	0.877	21.25	−721.0	348.3

3 RESULTS

Numerical experiments were conducted for core Rayleigh numbers in the range $10^4 \leq Ra_{\bar{\theta}} \leq 10^8$, and viscosity ratios up to $\Delta\mu = 10^6$. In Fig. 3, the Nusselt number is plotted as a function of the core Rayleigh number. The convective heat transfer weakens as the viscosity ratio increases. Moreover, the logarithmic slope β depends strongly on the value of $\Delta\mu$. According to our calculations, this slope ranges from 0.24 to 0.37 for $\Delta\mu = 10^2$ and 10^6, respectively. For small viscosity ratios ($\Delta\mu < 10^2$), variable viscosity calculations get closer to isoviscous laws at high Rayleigh numbers. For viscosity ratios equal to 10^3 and 10^4, a change in the value of β is observed (Fig. 3). The Rayleigh number at which the transition occurs increases with $\Delta\mu$. No transition is seen for $\Delta\mu = 10^5$ and $\Delta\mu = 10^6$, possibly because we did not reach high enough values

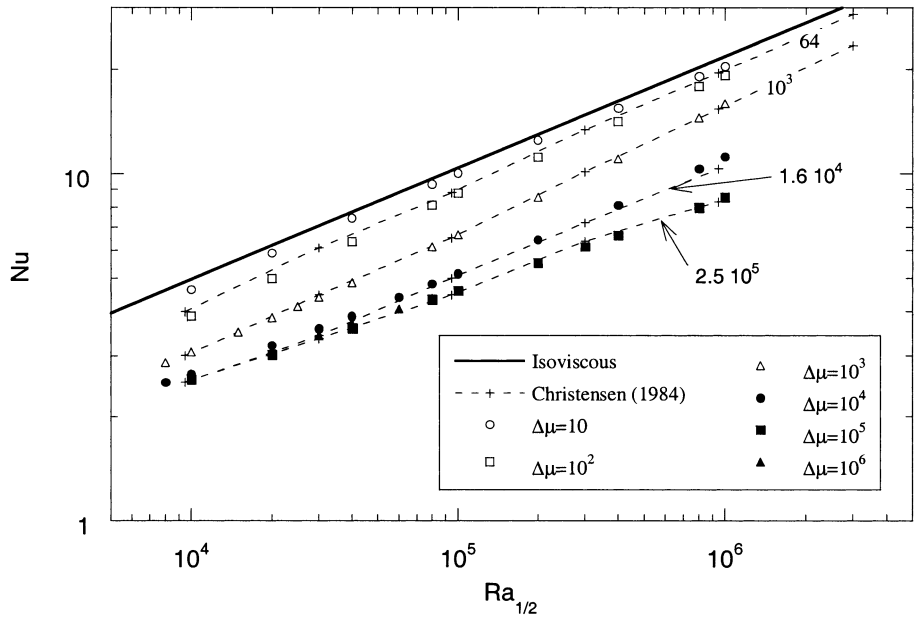

Figure 2. Comparison between the present study (white and black symbols) and the results of Christensen (1984) (crosses and dashed lines). For clarity, we have only represented Christensen's data for $\Delta\mu = 64$, 10^3, 1.6×10^4 and 2.5×10^5. The Nusselt number is plotted as a function of the median Rayleigh number ($Ra_{1/2}$). For comparison, the isoviscous scaling law is indicated by the bold line.

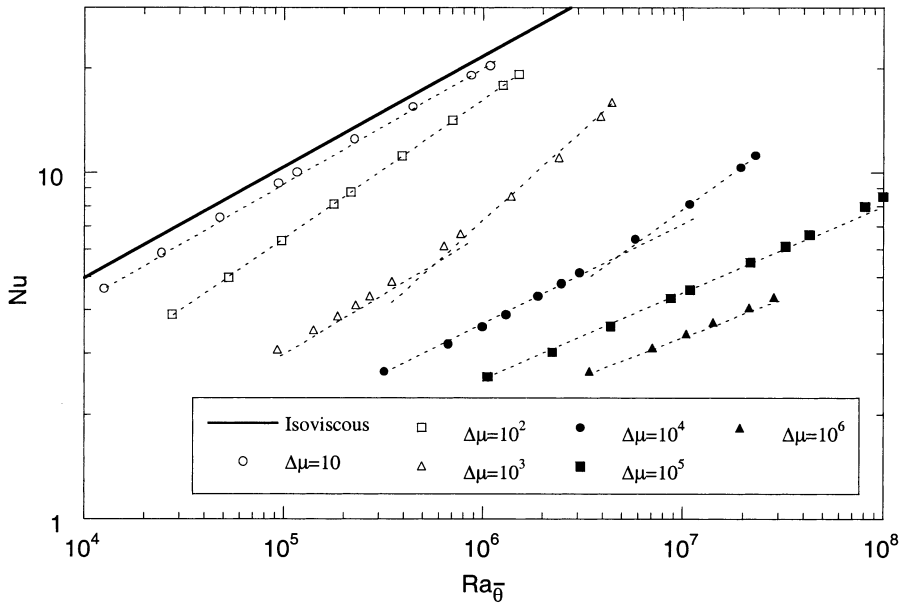

Figure 3. Heat flux as a function of the core Rayleigh number ($Ra_{\bar{\theta}}$), for several viscosity ratios ($\Delta\mu$).

of the Rayleigh number for these values of the viscosity ratio. The most likely interpretation of these results is that different regimes of convection occur, depending on both the Rayleigh number and the amplitude of the viscosity variations. Solomatov (1995) distinguishes three regimes: isoviscous convection, whole-layer convection (or intermediate regime), and conductive-lid convection. Solomatov (1995) and Moresi & Solomatov (1995) have proposed that the limit between the stagnant-lid regime and the intermediate regime does not depend on the Rayleigh number. They have estimated that the critical value of the viscosity contrast is about 10^4. The present results suggest that this limit also depends on the Rayleigh number (see Section 4.2).

3.1 Scaling law for the core temperature

The analytical models of Morris & Canright (1984) and Solomatov (1995) show that the temperature difference across the bottom thermal boundary layer is proportional to $1/\gamma$. A least-squares fit of data in Table 3(a) suggests that the non-dimensional temperature jump across the lower thermal boundary layer ($\delta\theta_1 = 1-\bar{\theta}$) is well described by (Fig. 4)

$$(1-\bar{\theta}) = \frac{c_1'}{\gamma} + c_2'$$

with

$$c_1' = 1.43 \pm 0.01 \quad \text{and} \quad c_2' = -0.03 \pm 0.01 . \tag{22}$$

The correlation coefficient reaches 97 per cent. A slight dispersion of $\delta\theta_1$ as a function of the Rayleigh number is observed and may be due to numerical uncertainties.

Although it is close to zero, the value of c_2' is significantly different from zero. Moreover, it is much larger than the standard deviation on temperature, which is equal to 0.005 at a maximum. Consequently, the viscosity ratio across the lower thermal boundary layer (ξ) decreases with increasing values of γ. Nataf (1991) noticed that the value of ξ should be less than 10. The present result suggests that it is even lower (around 3), and that it varies slightly with the viscous temperature scale.

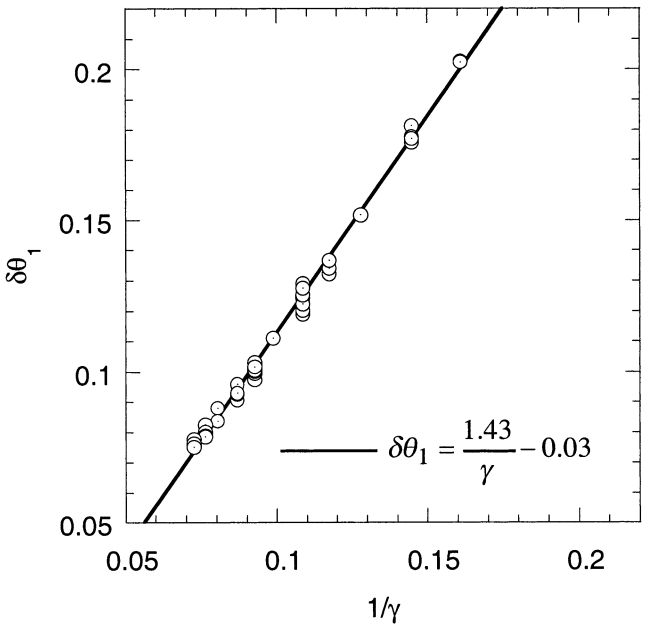

Figure 4. Determination of the temperature of the well-mixed interior ($\bar{\theta}$) as a function of the parameter γ.

3.2 Scaling law for the heat flux

3.2.1 Input data and inversion method

Inversions are performed for the runs listed in Table 3(a). All the calculations are conducted with an aspect ratio equal to 1, free-slip boundaries, and a viscosity ratio higher than 10^4. These runs fall into the conductive-lid regime, as defined by Moresi & Solomatov (1995). Some experiments with values of $Ra_{\bar{\theta}}$ larger than those reported in Table 3(a) were performed, but are not used in the present inversions because no stationary state was obtained.

The inversion method used in this study follows the method proposed by Tarantola & Valette (1982) to solve the generalized

Table 3(a). Numerical results for $\Delta\mu \geq 10^4$, when steady state has been reached. $\Delta\mu$ is the viscosity ratio, Ra_0 the surface Rayleigh number, $\bar{\theta}$ the temperature of the well-mixed interior, Nu the Nusselt number, $Ra_{\bar{\theta}}$ the core Rayleigh number, δ_{adv} the thickness of the conductive lid predicted by the method of the tangent through the inflexion point, and $\delta_{\Delta\Phi=0}$ the thickness of the conductive lid predicted by the comparison between advected and conducted heat flux.

$\Delta\mu$	Ra_0	$\bar{\theta}$	Nu	$Ra_{\bar{\theta}}$	δ_{adv}	$\delta_{\Delta\Phi=0}$
10^4	80	0.871	2.512	2.4×10^5	0.226	0.171
–	100	0.876	2.662	3.2×10^5	0.208	0.158
–	200	0.881	3.203	6.7×10^5	0.159	0.118
–	300	0.880	3.585	9.9×10^5	0.137	0.097
–	400	0.878	3.891	1.3×10^6	0.116	0.082
–	600	0.874	4.393	1.9×10^6	0.094	0.063
–	800	0.873	4.801	2.4×10^6	0.081	0.051
2.5×10^4	63.2	0.889	2.598	5.1×10^5	0.227	0.172
–	632.5	0.889	4.841	5.1×10^6	0.089	0.060
5×10^4	44.7	0.897	2.577	7.3×10^5	0.236	0.180
–	89.5	0.903	3.049	1.6×10^6	0.188	0.142
–	178.9	0.900	3.635	3.1×10^6	0.145	0.109
–	268.3	0.900	4.066	4.2×10^6	0.124	0.092
–	357.8	0.899	4.409	6.0×10^6	0.110	0.081
–	447.2	0.899	4.691	7.5×10^6	0.100	0.072
–	670.8	0.898	5.253	1.1×10^7	0.083	0.057
10^5	31.6	0.903	2.575	1.0×10^6	0.241	0.184
–	63.3	0.909	3.032	2.2×10^6	0.194	0.148
–	126.5	0.907	3.597	4.4×10^6	0.153	0.117
–	253.0	0.907	4.337	8.7×10^6	0.118	0.089
–	316.2	0.907	4.559	1.1×10^7	0.108	0.081
–	474.3	0.907	5.117	1.6×10^7	0.092	0.068
–	632.5	0.907	5.522	2.2×10^7	0.081	0.058
2.5×10^5	20.0	0.912	2.595	1.7×10^6	0.244	0.187
–	200.0	0.916	4.550	1.8×10^7	0.115	0.088
5×10^5	14.1	0.917	2.625	2.4×10^6	0.243	0.188
–	28.3	0.921	3.071	5.0×10^6	0.198	0.152
–	56.6	0.920	3.629	9.9×10^6	0.160	0.122
–	84.9	0.921	4.031	1.5×10^7	0.138	0.106
–	113.1	0.921	4.319	2.0×10^7	0.126	0.097
10^6	10	0.922	2.667	3.4×10^6	0.240	0.187
–	20	0.925	3.116	7.1×10^6	0.196	0.152
–	30	0.924	3.425	1.0×10^7	0.174	0.135
–	40	0.925	3.697	1.4×10^7	0.158	0.122

Table 3(b). As (a), but for viscosity ratios such that $5.10^2 < \Delta\mu < 10^4$.

$\Delta\mu$	Ra_0	$\bar{\theta}$	Nu	$Ra_{\bar{\theta}}$	δ_{adv}	$\delta_{\Delta\Phi=0}$
5×10^2	447.2	0.797	3.295	6.3×10^4	0.095	0.077
–	670.8	0.798	3.773	9.5×10^4	0.075	0.058
10^3	253.0	0.819	2.872	7.2×10^4	0.139	0.112
–	316.2	0.822	3.082	9.3×10^4	0.124	0.098
–	474.3	0.824	3.505	1.4×10^5	0.099	0.075
–	632.5	0.823	3.846	1.9×10^5	0.083	0.061
2.5×10^3	200.0	0.848	2.863	1.5×10^5	0.163	0.125
5×10^3	141.42	0.863	2.744	2.2×10^5	0.188	0.143
–	282.8	0.868	3.336	4.6×10^5	0.138	0.103
–	424.3	0.866	3.756	6.8×10^5	0.113	0.081
–	565.7	0.863	4.096	8.8×10^5	0.097	0.067

non-linear inversion problem using the least-squares criterion. A theoretical relation, or model, is first established among the data ($\bar{\theta}$ and Nu), the constants describing the physical problem (Ra and γ), and the parameters to be determined. In the solution proposed by Tarantola & Valette (1982), data and parameters are unknown quantities that have a small standard deviation for the data, and a very large (infinite) standard deviation for the parameters. The minimization of the least-squares criterion yields theoretical values of the data ($\bar{\theta}_{\mathrm{th}}$ and Nu_{th}) and theoretical values of the parameters. In addition, it provides an *a posteriori* covariance matrix. In this matrix, the variance on the data does not change, whereas the variance on the parameters has been reduced and yields the standard deviation. The *a posteriori* analysis of the discrepancy between the input data ($\bar{\theta}$ and Nu) and the inverted data ($\bar{\theta}_{\mathrm{th}}$ and Nu_{th}) is compared with the uncertainty on these data. It is an efficient way of checking the validity of the theoretical relationship (Sotin 1986). Using this method, two kinds of models have been tested for determining the scaling law between the Nusselt and Rayleigh numbers.

3.2.2 *Model 1*

The first model is deduced from the study of Davaille & Jaupart (1993) for a fluid heated from within. In this case, the temperature difference across the top thermal boundary layer, ΔT_{e}, is given by eq. (6). For a fluid heated from below, the dimensional analysis predicts a slight deviation from eq. (6). An approximation of ΔT_{e} as a function of the viscous temperature scale defined by eq. (7) is given by

$$\Delta T_{\mathrm{e}} = a\Delta T_{\mathrm{v}} + b\,, \tag{23}$$

where ΔT_{v} is given by eq. (7). This difference is due to the existence of a thermal boundary layer at the bottom of the fluid. The parameter b is not a constant and should depend on γ. The present inversion assumes that this dependence is weak. Finally, the consistency of (23) is controlled by the results of the inversion, which will show that this kind of law is not well constrained.

In the case of an exponential viscosity law (eq. 14), eq. (23) becomes

$$\theta_{\mathrm{c}} = \bar{\theta} - \left(\frac{c_1}{\gamma} + c_2\right), \tag{24}$$

where θ_{c} is the non-dimensional temperature at the bottom of the conductive lid. Parameters c_1 and c_2 must be determined by inverting the results of the numerical experiments.

It is then assumed that the viscosity jump across the convective sublayer is small, and that the scaling law relating the Rayleigh and Nusselt numbers of the convective sublayer (Ra_{SL} and Nu_{SL}) is a power law similar to that obtained for isoviscous fluids (eq. 4). The values for Ra_{SL} and Nu_{SL} are deduced from the values of the Rayleigh number and the Nusselt number of the whole cell ($Ra_{\bar{\theta}}$ and Nu), the temperature at the top of the lower thermal boundary (θ_{c}), and the non-dimensional lid thickness (δ_{c}):

$$\begin{aligned} Ra_{\mathrm{SL}} &= (1-\delta_{\mathrm{c}})^3(1-\theta_{\mathrm{c}})Ra_{\bar{\theta}}\,, \\ Nu_{\mathrm{SL}} &= \frac{(1-\delta_{\mathrm{c}})}{(1-\theta_{\mathrm{c}})}\,Nu\,. \end{aligned} \tag{25}$$

In the conductive lid, heat is transferred by conduction, and δ_{c} is given by

$$\delta_{\mathrm{c}} = \theta_{\mathrm{c}}/Nu\,. \tag{26}$$

Table 4. Chi-square and inverted values of the parameters for the various models proposed in this study.

Model	K^2	Parameters			
		a	β	c_1	c_2
1	11.7[(1)]	0.69 ± 0.2	0.276 ± 0.004	0.83 ± 0.5	-0.03 ± 0.01
–	12.5	0.51 ± 0.02	0.273 ± 0.004	1.5[(2)]	-0.05 ± 0.004
–	15.9	0.29 ± 0.02	0.268 ± 0.005	3.4[(2)]	-0.1 ± 0.006
		a	β	c	
2a	14.1	3.8 ± 0.2	0.258 ± 0.009	-1.63 ± 0.04	
2b	4.5	3.8 ± 0.3	0.260 ± 0.006	-1.64 ± 0.07	

Notes: [(1)] best fit of eq. (27). [(2)] The value of c_1 is fixed (see text, Section 4.3).

Finally, introducing (17) (24) (25) and (26) into (4) yields a scaling law of the Nusselt number as a function of the surface Rayleigh number:

$$Nu = a\left(1 - \frac{\bar{\theta} - c_1/\gamma - c_2}{Nu}\right)^{3\beta-1}\left(1 - \bar{\theta} + \frac{c_1}{\gamma} + c_2\right)^{\beta+1} \times \exp(\beta\gamma\bar{\theta}) Ra_0^{\beta}. \quad (27)$$

In this relation, a, β, c_1 and c_2 are parameters which must be determined by inverting the ($\bar{\theta}$, Nu) pairs. The best fit of eq. (27) is obtained for the set of values reported in the first line of Table 4. In order to obtain an acceptable value of the chi-square coefficient, the standard deviations of the Nusselt number and the core temperature must be $\sigma_{Nu} = 3$ per cent and $\sigma_{\bar{\theta}} = 0.5$ per cent, respectively. The inverted parameters provide a very good fit of the data (Fig. 5). However, parameters a and

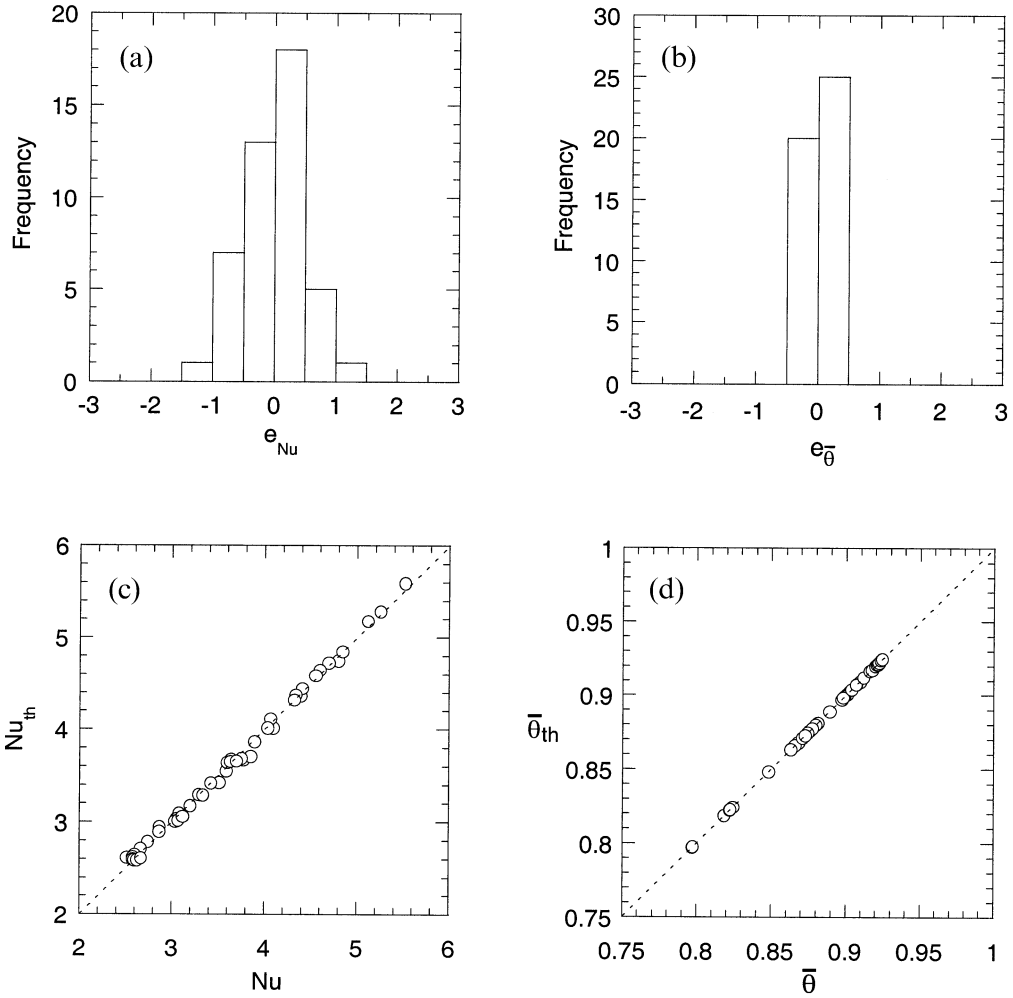

Figure 5. Model 1. Distribution of the relative errors on the Nusselt number (a) and on the temperature of the well-mixed interior (b). The relative error e_x of a datum x is defined by $e_x = (x - x_{th})/\sigma_x$, where x_{th} is the modelled value of x, and σ_x its standard deviation. Comparison between the numerical and modelled Nusselt numbers (c) and temperatures of the well-mixed interior (d).

c_1 (and, to a weaker extent, c_2) are poorly constrained. They are strongly correlated with each other, which means that they cannot be inverted independently. This could mean that the conductive lid cannot be separated from the upper thermal boundary layer. This observation led us to investigate a second model.

3.2.3 *Model 2*

The second model derives a scaling law for the whole layer of the fluid, including the conductive lid. As outlined by Christensen (1984), a second parameter is needed to describe the heat flux fully. The studies by Morris & Canright (1984) and Fowler (1985) suggest the following relationship:

$$Nu = a\gamma^c Ra_{\bar{\theta}}^{\beta}. \tag{28}$$

If the viscosity follows eq. (14), the parameter γ is given by eq. (15). The data in Table 3(a) were inverted following eq. (28), and the results are given in Table 4 (model 2a). With these coefficients, relation (28) fits the numerical results very well (Figs 6 and 7). The standard deviations required to give a coherent value of the chi-square coefficient are similar to those of model 1 (3 per cent on the Nusselt number and 0.5 per cent on the core temperature).

In order to check the consistency of eqs (22) and (28), another inversion was carried out assuming the core temperature to be given by eq. (22) (model 2b). The core temperature is now a constant; that is to say, $\bar{\theta}$ is fixed for each calculation. The parameters resulting from this inversion are nearly the same as those found for model 2a (Table 4).

Eq. (28) with the parameters of model 2 explains our numerical results with only 3 per cent error on Nu and 0.5 per cent on $\bar{\theta}$. The non-stationary runs (high values of the Rayleigh number and viscosity ratio larger than 10^4), which were not taken into account for inversion, fit well along the scaling relation (Fig. 7). Therefore, this relation may be extrapolated to higher values of the Rayleigh number.

4 DISCUSSION

We now discuss our results. First, we emphasize the efficiency of non-linear inversion to interpret the numerical data (Sections 4.1 and 4.2). Then, we use two different methods

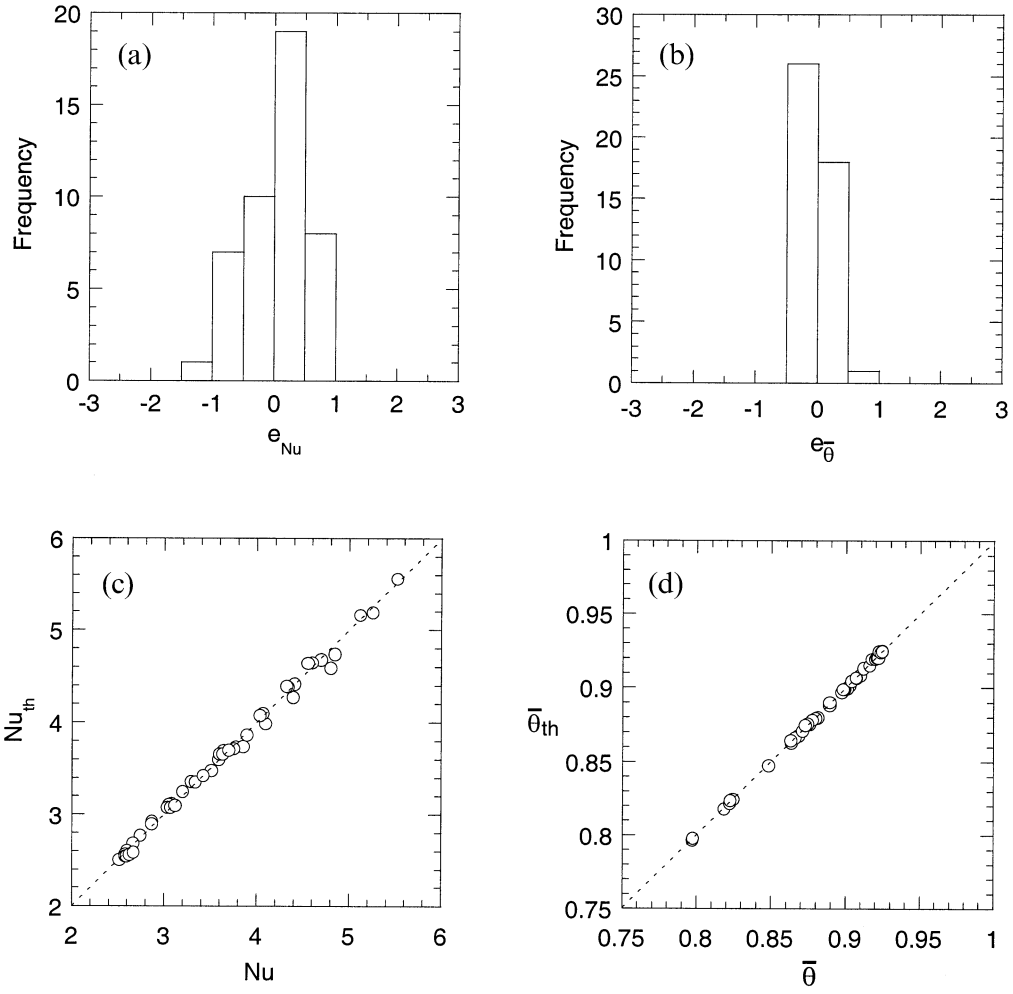

Figure 6. As Fig. 5, but for the model 2a.

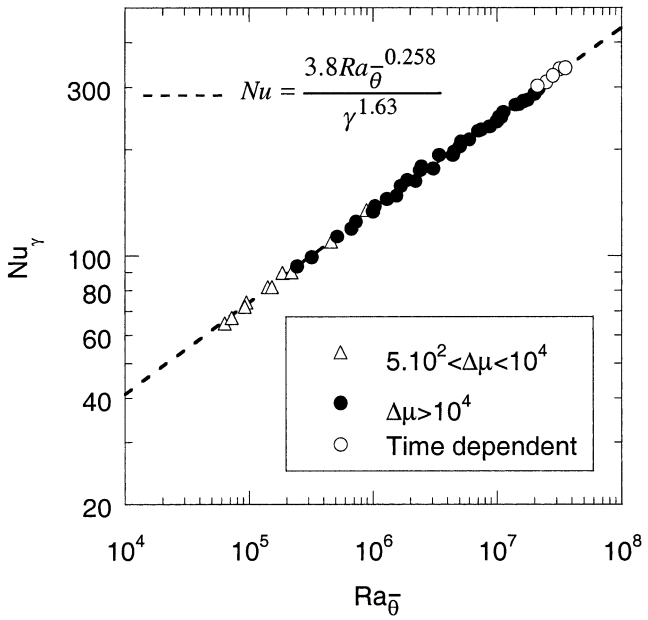

Figure 7. Scaling relation for the heat flux following model 2a. The length-scale is the whole thickness of the fluid. Note that the non-stationary solutions, which are represented by white circles, fit well along the parametrization. For clarity, we have represented the 'reduced' Nusselt number $Nu_\gamma = Nu\gamma^c$ (where $c = 1.63$), instead of the Nusselt number.

to show that the hypothesis of an isoviscous convective sublayer is not consistent with the experimental data (Sections 4.3 and 4.4).

4.1 Comparison with previous studies

Morris & Canright (1984) and Fowler (1985) have developed analytical models of Rayleigh–Bénard convection that include temperature-dependent viscosity. They both predict that heat flux follows a power law of the form (28), with $\beta = 0.2$. A similar value is expected for an isoviscous fluid limited by rigid top and bottom boundaries (Roberts 1979), although numerical experiments suggest slightly larger values (Table 1). Morris & Canright (1984) and Fowler (1985) have also computed theoretical values for a and c (Table 5). Moresi & Solomatov (1995) assume $\beta = 0.2$ to perform a least-squares fit of their data. They find $a = 1.89$ and $c = -1.02$, in agreement with the theoretical values found for the case of an infinite Rayleigh number (Fowler 1985). The present inverted values are different from these previous results.

Table 5. Theoretical and numerical values for the parameters of the scaling law (28). Moresi & Solomatov (1995) fixed the value of β to its theoretical value for an infinite Rayleigh number, and computed the other parameters using a least-squares fit of their data. In the present study, the three parameters are obtained from a generalized non-linear inversion.

Reference	a	β	c
Morris & Canright (1984)	1.822	0.2	−1.2
Fowler (1985)	2.043	0.2	−1.0
Moresi & Solomatov (1995)	1.89	0.2	−1.02
This study	3.8	0.258	−1.63

We have compared the scaling relation (28) with the results of Christensen (1984). Christensen only gives the mean temperature over the whole box. To estimate the values of his $Ra_{\bar{\theta}}$, we have therefore extrapolated the core temperature using eq. (22). The results are plotted in Fig. 8, together with our proposed scaling law (solid line). Clearly, the values we have proposed for the coefficients of eq. (28) also explain the calculations of Christensen (1984). We performed a similar comparison between the data of Christensen (1984) and the scaling relations proposed by Moresi & Solomatov (1995) (eqs 8 and 9). It turns out that the law suggested by Moresi & Solomatov (1995) does not provide a good fit of Christensen's data (Fig. 1). We want to emphasize that the results of 2-D convection numerical experiments ($\bar{\theta}$ and Nu) from Moresi & Solomatov (1995), Christensen (1984) and the present study are very close to each other. Therefore, the origin of the difference between the scaling law we propose and that suggested by Moresi & Solomatov (1995) may be related to the data processing. To obtain their scaling law, Moresi & Solomatov fix the parameter β to a theoretical value ($\beta = 0.2$). This theoretical value was obtained assuming an infinite Rayleigh number (Morris & Canright 1984; Fowler 1985). The values of the other parameters (a and c) are determined by a least-squares fit of the data. In the non-linear inversion, however, the three parameters are inverted simultaneously from the data. In particular, no theoretical value is assumed for β. According to the non-linear inversion, the experimental value of β (Table 5) is well constrained ($\sigma_\beta = 0.009$), and is 30 per cent higher than the theoretical value predicted for an infinite Rayleigh number.

The discrepancy between experimental and theoretical values of β may be due to the interaction between the top and bottom boundary layers. The plumes that form at each boundary modify the stability of the opposite thermal boundary layer as they reach it. Therefore, the conductive lid is eroded by the hot plume. Moreover, analytical studies assumed that the conductive lid is strictly stagnant. In fact, the lid is able to have a horizontal sliding, although this displacement is very small

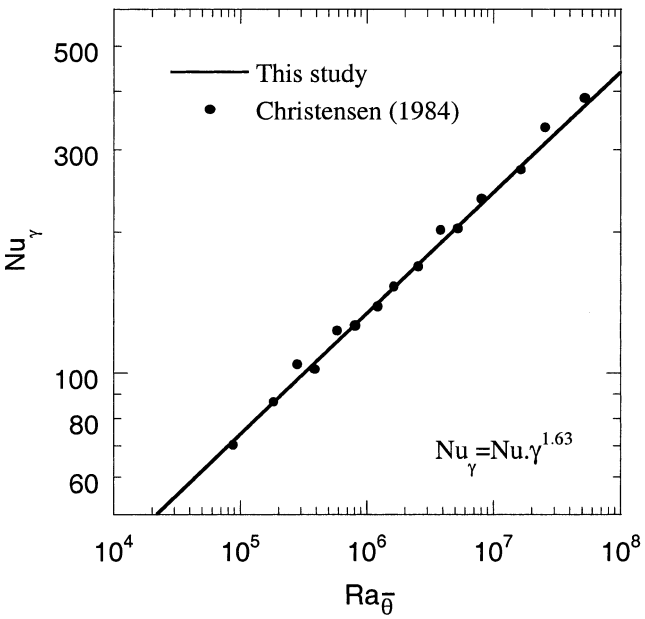

Figure 8. Comparison between the results of Christensen (1984) and the scaling law for heat flux proposed in the present study.

compared with the convective flow (Fowler 1985). We propose that the thermal erosion and the small sliding of the conductive lid explain the difference between the inverted and theoretical values of β.

4.2 A criterion for the conductive-lid regime

In their studies, Solomatov (1995) and Moresi & Solomatov (1995) assume that the boundary between the transitional and conductive-lid regimes does not depend on the value of the Rayleigh number. Using the study of Stengel *et al.* (1982), they locate this boundary for a viscosity contrast of about 10^4. One interesting feature of the inversion process is an analysis of the *a posteriori* difference between the inverted law and the data. In most cases, it allows the differentiation of sets of data falling into different regimes (Sotin 1986). In the present study, numerical experiments have also been conducted for viscosity ratios lower than 10^4 (Table 3b). These runs fit our model 2a well. Therefore, if the Rayleigh number is low enough, a conductive lid may also exist for low-viscosity contrasts ($5\times10^2<\Delta\mu<10^4$), and the limit between the transitional and conductive-lid regimes may depend on the Rayleigh number.

The formation of a lid requires the viscous friction near the surface to overcome the buoyancy. Therefore, the surface Rayleigh number (Ra_0) must be higher than a certain value (Ra_c) for convection to exist (Grasset & Parmentier 1998). The variations of Ra_c as a function of the amplitude of viscosity variations can be used to define the limit between the lid regime and the conductive-lid regime. For fluids whose viscosity follows eq. (14), Stengel *et al.* (1982) and Richter *et al.* (1983) proposed that Ra_c is approached by

$$Ra_c = 20.9\gamma^4 \exp(-\gamma/2). \tag{29}$$

A similar limit can be defined for the bottom Rayleigh number (Ra_1), which is computed with the viscosity at the base of the fluid:

$$Ra_{c,1} = 20.9\gamma^4 \exp(\gamma/2). \tag{30}$$

In Fig. 9, we have drawn the curve defined by eq. (30). The limit proposed by Moresi & Solomatov (1995) is also shown.

The experiments of Moresi & Solomatov (1995) conducted at bottom Rayleigh numbers equal to 10^7 and 10^8 had very large viscosity ratios, leading to surface Rayleigh numbers lower than 100. Such values are lower than the critical values defined by eq. (30), and the transition towards the transitional regime could not be observed in their numerical experiments.

The present study supports the fact that the convective-lid regime exists at small viscosity ratios for small values of the bottom Rayleigh number. For instance, a viscosity ratio of 500 yields a conductive lid if the bottom Rayleigh number is smaller than 10^6. On the other hand, viscosity ratios larger than 10^4 are required for bottom Rayleigh numbers larger than 10^7. However, one cannot be sure that the limit between the transitional regime and the conductive-lid regime proposed in the present study can be extrapolated to very high values of the Rayleigh number. Following theoretical studies at infinite values of the Rayleigh number, this boundary does not depend on the Rayleigh number. It may be described by $\Delta\mu=10^4$, as proposed by Moresi & Solomatov (1995).

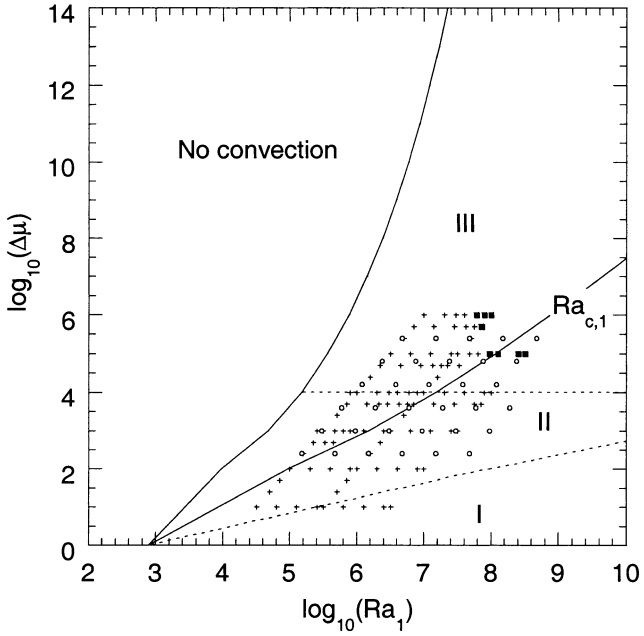

Figure 9. Location of the various regimes. I: whole-layer convection; II: transitional regime; III: conductive-lid regime. Boundaries between these regimes are shown. Dotted lines are from Solomatov (1995). The boundary between II and III proposed in this study is indicated by the curve labelled $Ra_{c,1}$. Our numerical experiments are represented by crosses (black points if they are not stationary). White circles are the points of Christensen (1984).

4.3 Thermal boundary layer analysis

Linear stability analysis performed for isoviscous fluids with free-slip boundaries predicts that the upper and lower thermal boundary layer Rayleigh numbers ($Ra_{\delta,\mathrm{top}}$ and $Ra_{\delta,\mathrm{bot}}$, respectively) are equal and do not depend on the Rayleigh number. For an aspect ratio equal to 1, $Ra_\delta \sim 2.46$. However, experimental and numerical studies have observed a slight dependence on the Rayleigh number due to the fact that the logarithmic slope is not exactly 1/3 (e.g. Sotin & Labrosse 1999). The present calculations (Table 1) fit the relation $Ra_\delta = 3.64Ra^{0.037}$ (line 2 in Fig. 10) well. For a fluid with mixed boundary conditions (rigid on top and free-slip at the bottom), a stronger dependence is expected. The core temperature is greater than 0.5 and depends slightly on the Rayleigh number: $\bar{\theta}=0.54Ra^{0.018}$. The system is no longer symmetric, and the top and bottom thermal boundary layers do not behave similarly. The relation that describes $Ra_{\delta,\mathrm{bot}}$ is close to that found for two free-slip boundaries, whereas $Ra_{\delta,\mathrm{top}}$ depends more strongly on the Rayleigh number (line 1 in Fig. 10): $Ra_{\delta,\mathrm{top}}=2.28Ra^{0.319}$. A rigid surface inhibits convective instabilities, and larger temperature variations are required for downwelling instabilities to form.

Eq. (3) can also be written for a variable viscosity fluid. Using the non-dimensional parameters, the Rayleigh numbers of the upper and lower thermal boundary layer are

$$\text{top:}\ Ra_\delta = \frac{(\bar{\theta}-\theta_c)^4}{Nu^3}\, Ra_{\bar{\theta}}, \tag{31}$$

$$\text{bottom:}\ Ra_\delta = \frac{(1-\bar{\theta})^4}{Nu^3}\, Ra_{\bar{\theta}}, \tag{32}$$

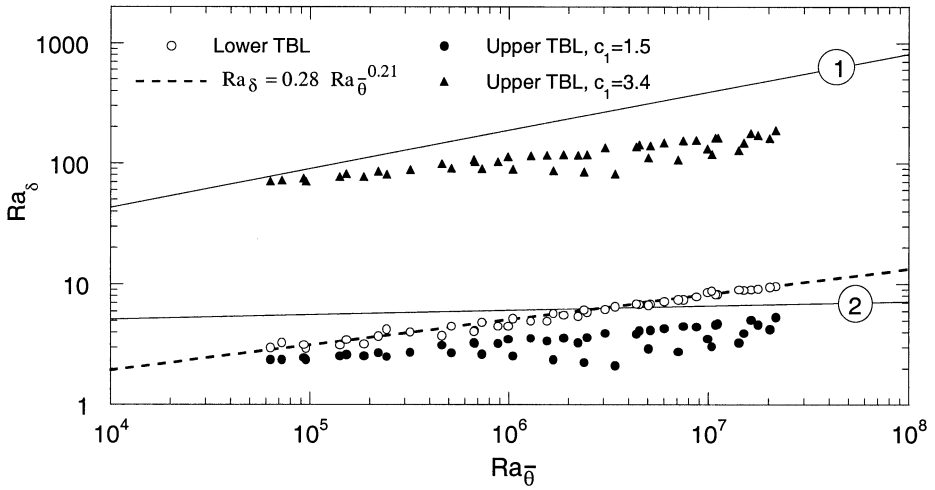

Figure 10. Upper ($Ra_{\delta,\mathrm{top}}$) and lower ($Ra_{\delta,\mathrm{bot}}$) thermal boundary layer Rayleigh numbers as a function of the core Rayleigh number ($Ra_{\bar\theta}$), according to model 1. The lines labelled 1 and 2 represent the relation between $Ra_{\delta,\mathrm{top}}$ and Ra, in the case of an isoviscous fluid with a rigid surface and a free-slip surface, respectively. The values of $Ra_{\delta,\mathrm{bot}}$ (white circles) do not depend on c_1 and fit relation (33) (dashed line) well. Two values of c_1 are considered to compute $Ra_{\delta,\mathrm{top}}$: $c_1 = 1.5$ (black circles), and $c_1 = 3.4$ (black triangles).

where θ_c is the non-dimensional temperature at the base of the conductive lid. One difficulty is the determination of the thickness of the conductive lid (δ_c, eq. 26). Indeed, the results of the previous inversion show that the transition between the top thermal boundary layer and the conductive lid is fuzzy, since the standard deviations of c_1 and c_2 are very large. The following discussion is based on the determination of scaling relations between the thermal boundary layer Rayleigh numbers and the core Rayleigh number (Fig. 10). In the isoviscous case, previous studies (Bergholz *et al.* 1979; Sotin & Labrosse 1999) have used a far-field Rayleigh number (Ra^+) for each half of the box. In the case of a fluid with strong viscosity variations, the definition and the meaning of Ra^+ are less obvious. For clarity, we prefer to use the core Rayleigh number. This does not change the interpretation of the thermal boundary layer analysis.

4.3.1 *Lower thermal boundary layer*

In the case of the conductive-lid regime, the temperature difference across the lower thermal boundary layer depends on γ (eq. 22). For a given value of γ, a slight dispersion for different values of the Rayleigh number is observed, but it is smaller than the standard deviation on the mean temperature.

The development of hot instabilities, which form at the lower thermal boundary layer, is enhanced by the decrease of viscosity across the boundary, leading to a temperature difference across the boundary layer smaller than that in the isoviscous case (Rayleigh–Bénard convection). In the following calculations, the temperature difference is given by the scaling relation (22). Whatever the value of c_1, the value of $Ra_{\delta,\mathrm{bot}}$ is close to that obtained in the case of an isoviscous fluid with free-slip boundaries (Fig. 10), although the dependence on the core Rayleigh number is larger. By computing $Ra_{\delta,\mathrm{bot}}$ with eq. (32), the data in Table 3(a) fit the relation

$$Ra_{\delta,\mathrm{bot}} \sim 0.28 Ra_{\bar\theta}^{0.21} \tag{33}$$

well (dashed line in Fig. 10). Consequently, the characteristics of the bottom thermal boundary layer (thickness, temperature variations) cannot be described by scaling laws based on results for an isoviscous fluid. Scaling laws (22) and (33) are more relevant.

4.3.2 *Top thermal boundary layer*

According to Morris & Canright (1984), the temperature difference across the top thermal boundary layer is about three times larger than that across the lower thermal boundary layer. However, the inversion performed in the present study does not constrain the boundary between the conductive lid and the top thermal boundary layer. At the limit between the lid and the top thermal boundary layer, viscosity is higher and inhibits the formation of a cold instability. Most of the viscosity variations occur within the conductive lid and the top thermal boundary layer. Therefore, the value of $Ra_{\delta,\mathrm{top}}$ depends strongly on the thickness of the conductive lid.

Since the standard deviation on the inverted value of c_1 is large, we have considered two possible sets of parameters (Table 4) to simulate two possible dynamic patterns (isoviscous fluid with either free-slip or rigid boundary). Note that the solution having the minimal value of chi-square ($c_1 = 0.83$) does not lie between these two end-member models, and yields very small values of the thermal boundary layer Rayleigh number.

The first set of parameters assumes $c_1 = 1.5$, in order to simulate the values obtained for the lower thermal boundary layer (line 2 in Fig. 10). In this case, the top and bottom thermal boundary layers have the same thermal amplitude. The values of $Ra_{\delta,\mathrm{top}}$ are close to, but smaller than, those obtained for the isoviscous case with free-slip boundary conditions (Fig. 10). Moreover, the dependence on the core Rayleigh number is stronger than that for the isoviscous case.

The second set of parameters assumes $c_1 = 3.4$ and was used to provide values of $Ra_{\delta,\mathrm{top}}$ close to those obtained for an isoviscous fluid with rigid boundary conditions at the surface (Fig. 10). Eqs (24) and (26) allow the determination of the thickness of the conductive lid (δ_{lid}). For $c_1 = 3.4$, the conductive lid is thinner than in the previous case ($c_1 = 1.5$), and consequently the viscosity jump across the sublayer is slightly

higher. On the other hand, the values of $\delta_{\rm lid}$ for $c_1=3.4$ are close to those computed with the law of Davaille & Jaupart (1993) ($\delta_{\rm DJ}$), which are obtained with $c_1=2.24$ and $c_2=0$ (Fig. 13). The values of $Ra_{\delta,\rm top}$ are close to those for an isoviscous fluid with a rigid surface, with some dispersion and smaller Ra dependence. This solution, if one accepts the validity of the viscous temperature scale, provides a better comparison with the isoviscous case (Fig. 10), but is unfortunately not the one obtained by the inversion of the data (model 1 with $c_1=0.83$).

Thermal boundary layer analysis suggests that the limit between the lid and the top thermal boundary layer is not well determined. It may be considered that the conductive lid is the continuation of the top thermal boundary layer. In addition, the lower thermal boundary layer seems to be more unstable than the upper one and may drive the convection process. Finally, the scaling law (33), which relates the bottom thermal boundary layer Rayleigh number to the core Rayleigh number, is useful for planetary applications. This relation can be used to assess the thickness of the lower thermal boundary layer and the heat flux across the fluid layer.

4.4 Thermal erosion of the conductive lid

Here, we propose two alternative methods to determine the mean thickness of the conductive lid ($\delta_{\rm lid}$). First, we use a graphical method based on the variations of the mean vertically advected heat flux ($\bar{\Phi}_z$) as a function of depth (Fig. 11). In the case of a fluid heated from within, the thickness of the conductive lid determined by this method is equal to that predicted by the viscous temperature scale (Davaille & Jaupart 1993). The second method is based on the comparison between the advected ($\Phi_{\rm adv}$) and conducted ($\Phi_{\rm cond}$) heat fluxes. The difference $\Delta\Phi=(\Phi_{\rm adv}-\Phi_{\rm cond})$ indicates which mechanism of heat transfer is dominant (Fig. 12). The depth at which convection balances conduction ($\Delta\Phi=0$) has very small lateral variations. The central uplift is related to lateral advection within the top thermal boundary layer. We propose that the value of $\delta_{\rm lid}$ is equal to the minimum depth reached by the

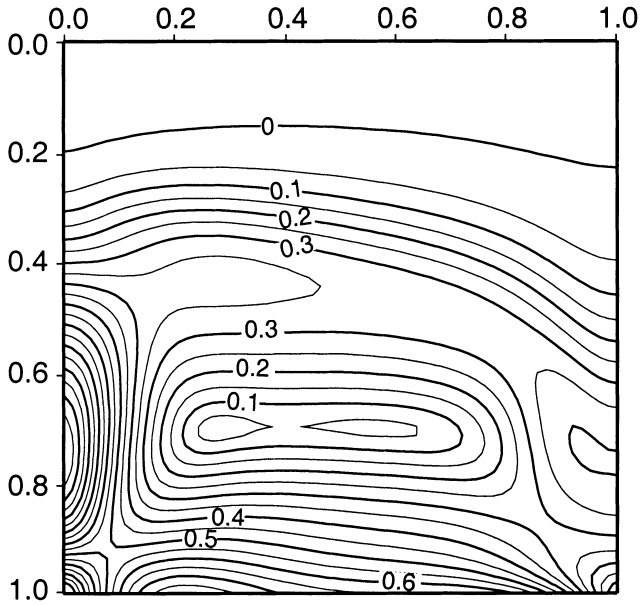

Figure 12. Difference between the total advected and conducted heat fluxes ($\Delta\Phi$), in the case $\Delta\mu=10^4$ and $Ra_{\bar{\eta}}=3.2\times10^5$. The depth of the conductive lid is defined by the minimal depth of the curve $\Delta\Phi=0$; that is, at the top of the central uplift.

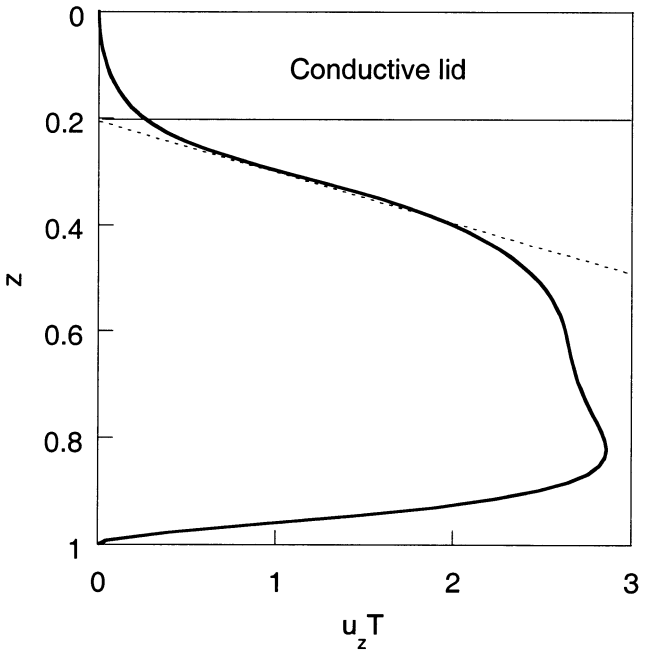

Figure 11. Mean vertical advective heat flux as a function of depth, in the case $\Delta\mu=10^4$ and $Ra_{\bar{\eta}}=3.2\times10^5$. The thickness of the conductive lid is determined by the depth at which the tangent through the inflexion point intersects the zero heat-flux axis (Davaille & Jaupart 1993).

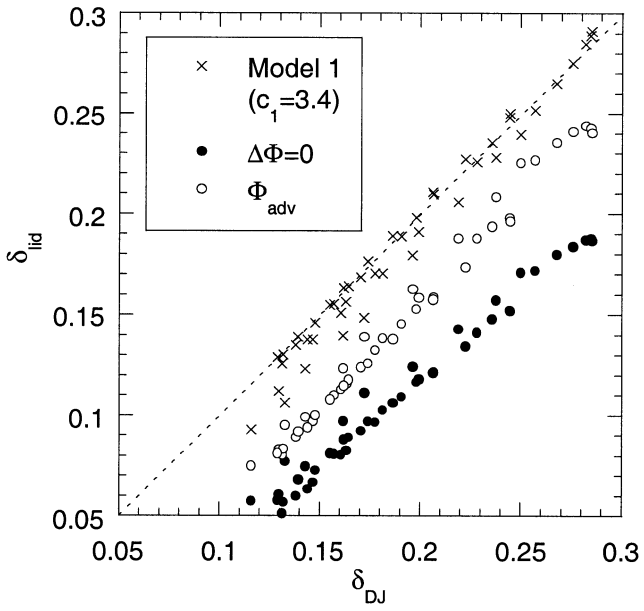

Figure 13. Thickness of the conductive lid predicted by the method of the tangent through the inflexion point (white circles) and by a comparison between the advected and conducted heat fluxes (black circles), as a function of the thickness of the non-eroded conductive lid ($\delta_{\rm DJ}$). $\delta_{\rm DJ}$ is computed by model 1 with $c_1=2.24$ and $c_2=0$ (Davaille & Jaupart 1993). The crosses represent the thickness predicted by model 1 with $c_1=3.4$ and $c_2=-0.1$.

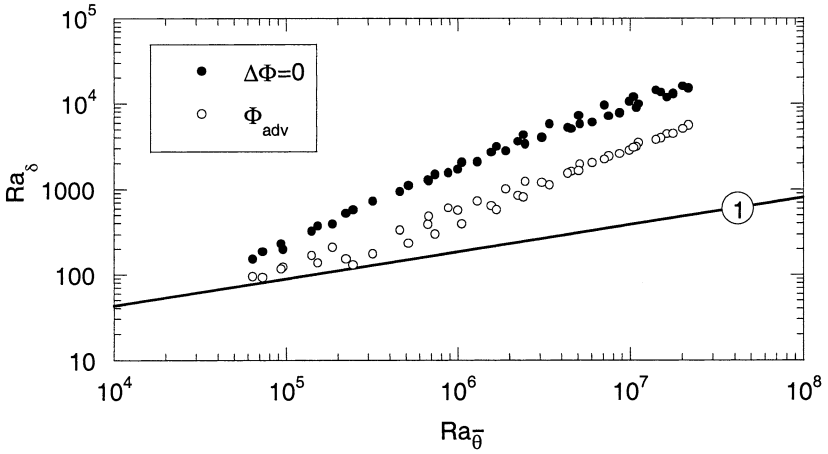

Figure 14. Upper thermal boundary layer Rayleigh number as a function of the core Rayleigh number, predicted by the method of the tangent through the inflexion point (white circles) and by a comparison between the advected and conducted heat fluxes (black circles).

curve $\Delta\Phi = 0$. Because small horizontal motions are possible at the base of the lid, this method may underestimate the value of $\delta_{\rm lid}$. At the top of the upper thermal boundary layer, however, $\bar{\Phi}_z$ is not a straight line, and the first method may overestimate the value of $\delta_{\rm lid}$. Therefore, the thickness of the conductive lid should lie between the values computed by theses two alternative methods.

The lid thickness computed by these methods is always smaller than that predicted by the scaling law of Davaille & Jaupart (1993) and by our model 1 (isoviscous rigid boundary with $c_1 = 3.4$) (Fig. 13). The thinning of the conductive lid may be related to thermal erosion induced by the hot plume. In a fluid heated from within, there are no hot plumes, and therefore no thermal erosion. This would explain why a viscous temperature scale allows the determination of the conductive lid in the case of a fluid heated from within, whereas it does not in the case of a fluid heated from below. Moreover, the values of $Ra_{\delta,\rm top}$ predicted by the alternative methods are larger than in the case of an isoviscous fluid with a rigid surface (Fig. 14). In other words, the upper thermal boundary layer is less unstable than that of an isoviscous fluid with a rigid surface.

5 CONCLUSIONS

Although the present study does not consider all the complexities that exist in a real mantle, it takes into account one major parameter, namely the temperature-dependent viscosity. Such a study leads a better understanding of the role of this parameter. The results from numerical experiments are in good agreement with previous studies. Different regimes of convection are observed, depending on the Rayleigh number and on the amplitude of the viscosity variations. The limit between the conductive-lid regime and the transitional regime depends on the value of the surface Rayleigh number and on the global viscosity ratio. In the case of the conductive-lid regime, the parameters of the scaling law for heat flux (eq. 28) are determined by a non-linear inversion of the numerical data. Therefore, they fit the experimental data sets independently of any prescribed theoretical value.

Thermal boundary layer analysis shows that, in the case of a fluid heated from below, the stability of thermal boundary layers is completely different from the case of a fluid heated from within (Davaille & Jaupart 1993). In the conductive-lid regime, convection is controlled by the instability in the lower thermal boundary layer. Moreover, the convective sublayer cannot be considered as an isoviscous fluid. The temperature difference across this layer can be calculated simply as a function of the viscous temperature scale (eq. 22). The heat flux can be determined with the help of a scaling law between the lower thermal boundary layer Rayleigh number and the core Rayleigh number (eq. 33). The thickness of the conductive lid is smaller than that predicted by the viscous temperature scale, suggesting that this layer is eroded by hot plumes coming from instabilities in the lower thermal boundary. Therefore, interactions between the thermal boundary layers play an important role in the stability of these layers.

ACKNOWLEDGMENTS

The research reported was supported by French CNRS-INSU grant 'Intérieur de la Terre'. We acknowledge the very constructive remarks of L.-N. Moresi and another anonymous reviewer, which allowed us to make significant improvements on the first version of this paper.

REFERENCES

Bergholz, R.F., Chen, M.M. & Cheung, F.B., 1979. Generalization of heat-transfer results for turbulent free convection adjacent to horizontal surfaces, *Int. J. Heat Mass Transfer,* **22,** 763–769.

Booker, J.R. & Stengel, K.C., 1978. Further thoughts on convective heat transport in a variable-viscosity fluid, *J. Fluid Mech.,* **86,** 289–291.

Chopra, P.N. & Paterson, M.S., 1984. The role of water in the deformation of dunite, *J. geophys. Res.,* **89,** 7861–7876.

Christensen, U.R., 1984. Heat transport by variable viscosity convection and implications for the Earth's thermal evolution, *Phys. Earth planet. Inter.,* **35,** 264–282.

Davaille, A. & Jaupart, C., 1993. Transient high-Rayleigh-number thermal convection with large viscosity variations, *J. Fluid Mech.,* **253,** 141–166.

Fowler, A.C., 1985. Fast thermoviscous convection, *Stud. appl. Math.,* **72,** 189–219.

Frick, H., Busse, F.H. & Clever, R.M., 1983. Steady three-dimensional convection at high Prandtl numbers, *J. Fluid Mech.,* **127,** 141–153.

Grasset, O. & Parmentier, E.M., 1998. Thermal convection in a volume trically heated, infinite Prandtl number fluid with strongly temperature-dependent viscosity: implications for planetary thermal evolution, *J. geophys. Res.,* **103,** 18 171–18 181.

Hansen, U. & Yuen, D.A., 1993. High Rayleigh number regime of temperature-dependent viscosity convection and the Earth's early thermal history, *Geophys. Res. Lett.,* **20,** 2191–2194.

Howard, L.N., 1966. Convection at High Rayleigh Number, in *Proc. 11th Int. Cong. Applied Mechanics*, pp. 1109–1115, ed. Gortler, H., Springer-Verlag, New York.

Jarvis, G.T. & Peltier, W.R., 1982. Mantle convection as a boundary layer phenomenon, *Geophys. J. R. astr. Soc.,* **68,** 389–427.

Karato, S.-I., Paterson, M.S. & Fitzgerald, J.D., 1986. Rheology of synthetic olivine aggregates: influence of grain size and water, *J. geophys. Res.,* **91,** 8151–8176.

Kvernvold, O., 1979. Rayleigh–Bénard convection with one free and one rigid boundary, *Geophys. astrophys. Fluid Dyn.,* **12,** 273–294.

Moresi, L.-N. & Solomatov, V.S., 1995. Numerical investigation of 2D convection with extremely large viscosity variations, *Phys. Fluids,* **7,** 2154–2162.

Morris, S. & Canright, D., 1984. A boundary-layer analysis of Bénard convection in a fluid of strongly temperature-dependent viscosity, *Phys. Earth plant. Inter.,* **36,** 355–373.

Nataf, H.-C., 1991. Mantle convection, plates, and hotspots, *Tectonophysics,* **187,** 361–371.

Ogawa, M., Schubert, G. & Zebib, A., 1991. Numerical simulations of three-dimensional thermal convection in a fluid with strongly temperature-dependent viscosity, *J. Fluid Mech.,* **233,** 299–328.

Parmentier, E.M., Sotin, C. & Travis, B.J., 1994. Turbulent 3D thermal convection in an infinite Prandtl number, volumetrically heated fluid: implications for mantle dynamics, *Geophys, J, Int.,* **116,** 241–251.

Richter, F.M., Nataf, H.-C. & Daly, S.F., 1983. Heat transfer and horizontally averaged temperature of convection with large viscosity variations, *J. Fluid Mech.,* **129,** 173–192.

Roberts, G.O., 1979. Fast viscous Bénard convection, *Geophys. astrophys. Fluid Dyn.,* **12,** 235–272.

Schubert, G. & Anderson, C.A., 1985. Finite element calculations of very high Rayleigh number thermal convection, *Geophys. J. R. astr. Soc.,* **80,** 575–601.

Schubert, G. & Spohn, T., 1992. Thermal history of Mars and the sulfur content of its core, *J. geophys. Res.,* **95,** 14 095–14 104.

Schubert, G., Cassen, P. & Young, R.E., 1979. Subsolidus convective cooling of terrestrial planets, *Icarus,* **38,** 192–211.

Solomatov, V.S., 1995. Scaling of temperature- and stress-dependent viscosity convection, *Phys. Fluids,* **7,** 266–274.

Sotin, C., 1986. Contribution à l'étude de la structure et de la dynamique interne des planètes, *PhD thesis,* University of Paris VII, Paris.

Sotin, C. & Labrosse, S., 1999. Three-dimensional thermal convection in an isoviscous, infinite Prandtl number fluid heated from within and from below: applications to heat transfert through planetary mantles, *Phys. Earth planet. Inter.,* **112,** 171–190.

Sotin, C., Parmentier, E.M., Carey-Gailhardis, E. & Stocklet, P., 1995. A 3-D multigrid Poisson solver on connexion machine: application to the convection within planetary interiors, in *Proc. 2nd European CM Users Mtg,* eds Alimi, J.M., Serna, A. & Scholl, M., Meudon-Paris, France.

Spalding, D.B., 1972. A novel finite difference formulation for differential expressions involving both first and second derivatives, *Int. J. num. Meth. Engng,* **4,** 551–559.

Stengel, K.C., Oliver, D.S. & Booker, J.R., 1982. Onset of convection in a variable-viscosity fluid, *J. Fluid Mech.,* **120,** 411–431.

Stevenson, D.J., Spohn, T. & Schubert, G., 1983. Magnetism and thermal evolution of terrestrial planets, *Icarus,* **54,** 466–489.

Stüben, K. & Trottenberg, U., 1982. Multigrids methods: fundamental algorithms, model problem analysis and applications, in *Multigrid Methods*, pp. 1–175, eds Hackbusch, W. & Trottenberg, U., Springer-Verlag, New York.

Tarantola, A. & Valette, B., 1982. Generalized nonlinear inverse problems solved using the least square criterion, *Rev. Geophys. Space Phys.,* **20,** 219–232.

Turcotte, D.L. & Oxburgh, E.R., 1967. Finite amplitude convective cells and continental drift, *J. Fluid Mech.,* **28,** 29–42.